Biochimica et Biophysica Acta 1808 (2011) 2629–2637

Contents lists available at ScienceDirect

Biochimica et Biophysica Acta

journal homepage: www.elsevier.com/locate/bbamem

Structural characterization of the interaction of the polyene antibiotic Amphotericin B with DODAB bicelles and vesicles

Tiago R. Oliveira, Carlos R. Benatti, M. Teresa Lamy *

Instituto de Física, Universidade de São Paulo, CP 66318, CEP 05314-970, São Paulo, SP, Brazil

ARTICLE INFO

Article history:
Received 29 March 2011
Received in revised form 27 July 2011
Accepted 28 July 2011
Available online 3 August 2011

Keywords:
Amphotericin B
DODAB
Spin label
DSC
Optical spectrum
Drug carrier

ABSTRACT

Amphotericin B (AmB) is widely used in the treatment of systemic fungal infections, despite its toxic effects. Nephrotoxicity, ascribed as the most serious toxic effect, has been related to the state of aggregation of the antibiotic. In search of the increase in AmB antifungal activity associated with low toxicity, several AmB-amphiphile formulations have been proposed. This work focuses on the structural characterization of a specific AmB formulation: AmB associated with sonicated dioctadecyl dimethylammonium bromide (DODAB) aggregates. Here, it was confirmed that sonicated DODAB dispersion is constituted by DODAB bicelles, and that monomeric AmB is much more soluble in bicelles than in DODAB vesicles. A new optical parameter is proposed for the estimation of the relative amount of amphiphile-bound monomeric AmB. With theoretical simulations of the spectra of spin labels incorporated in DODAB bicelles it was possible to prove that monomeric AmB binds preferentially to lipids located at the edges of DODAB bicelles, rigidifying them, and decreasing the polarity of the region. That special binding of monomeric AmB along the borders of bicelles, where the lipids are highly disorganized, could be used in the formulation of other carriers for the antibiotic, including mixtures of natural lipids which are known to form bicelles.

1. Introduction

The polyene antibiotic Amphotericin B (AmB) is one of the oldest and most widely used drugs for the treatment of systemic fungal infections [1–3]. It is supposed to act at the membrane level, altering the cell membrane permeability, a direct consequence of transmembrane pore formation [4–6]. It has also been suggested that AmB mechanism of action could be related to auto-oxidation with subsequent production of free radicals [7–9]. However, it presents several side effects, including nephrotoxicity and hemolytic activity, which limit the antibiotic use. Therefore, much effort has been devoted for developing different formulations, such as liposomal drug delivery systems, to reduce the antibiotic toxicity and increase its therapeutic effect [10,11].

Several studies have pointed out that AmB fungi membrane affinity, as well as antibiotic toxicity, are strongly dependent on the AmB aggregation state [12,13]. For instance, the main nephrotoxicity effect associated with the commercial formulation Fungizone, a mixed micelle of sodium deoxycholate and AmB, has been attributed to the low micellar stability for intravenous administration, which allows the formation of large AmB aggregates [14,15]. Accordingly, the monomeric state of AmB is usually ascribed as a low toxic form of the antibiotic [16,17]. Hence, to reduce the antibiotic toxicity, it is an interesting strategy to make AmB pharmaceutical formulations with the predominance of the monomeric form, even after dilution in the blood plasma. In this context, a formulation was proposed with sonicated aqueous dispersion of the cationic amphiphile dioctadecyl dimethylammonium bromide (DODAB), where AmB was predominantly found in the monomeric state [18]. This AmB–DODAB formulation was indeed found to be less nephrotoxic [19].

DODAB aqueous dispersion, prepared by simply mixing the amphiphile in water ($DODAB^{NS}$), was reported to form large unilamellar vesicles, with a very cooperative gel–fluid bilayer main transition around 42 °C (T_m) (see, for instance, [20]). After sonication, DODAB dispersion ($DODAB^{S}$) was found to be constituted by small particles, possibly bilayer fragments (bicelles) [21–23]. Using spin labels incorporated in aggregates present in $DODAB^{S}$ dispersion, it was possible to show the coexistence of gel and fluid domains bellow T_m. The data was interpreted as an indication of the presence of amphiphilic bicelles, where molecules in the gel state, in the bilayer fragment, coexist with fluid molecules, at the bilayer edges [22]. That was later confirmed by H NMR [24]. Hence, the monomeric solubilization of AmB into $DODAB^{S}$ dispersion [18] could be attributed to the presence of disordered amphiphiles around the borders of the bicelle, which would favor the adsorption of the drug as a monomer.

The purpose of the present work was a thorough structural characterization of the AmB–DODAB sonicated formulation, to help in

Abbreviations: (AmB), Amphotericin B; (DODAB), dioctadecyl dimethylammonium bromide; ($DODAB^{NS}$), Non-sonicated DODAB dispersion; ($DODAB^{S}$), sonicated DODAB dispersion; (ESR), Electron Spin Resonance; (DPPG), dipalmitoyl phosphatidylglycerol; (DPPC), dipalmitoyl phosphatidylcholine; (5- and 16-MESL), spin labels 5- and 16-doxyl stearic acid methyl ester derivatives

* Corresponding author. Tel.: +55 11 30916829; fax: +55 11 38134334.
E-mail address: mtlamy@if.usp.br (M.T. Lamy).

0005-2736
doi:10.1016/j.bbamem.2011.07.042

the understanding of the biological action of this formulation, and, possibly, in the development of new AmB carriers. Apart from monitoring the optical absorption spectrum of AmB, and the calorimetric behavior of DODAB aggregates, by differential scanning calorimetry (DSC), Electron Spin Resonance (ESR) spectra of spin labels incorporated in the amphiphilic aggregates were analyzed.

2. Materials and methods

2.1. Materials

Dioctadecyl dimethylammonium bromide (DODAB), Amphotericin B (AmB) and spin labels 5- and 16-doxyl stearic acid methyl ester derivatives (5- and 16-MESL) were purchased from Sigma-Aldrich (St Louis, MO, USA). The lipids dipalmitoyl phosphatidylglycerol (DPPG) and dipalmitoyl phosphatidylcholine (DPPC) were purchased from Avanti Polar Lipids (Birmingham, AL, USA). Milli-Q Plus water (Millipore) was used throughout. Chemical structures of DODAB, AmB, 5- and 16-MESL are presented in Fig. 1.

2.2. DODAB dispersions preparation

Non-sonicated DODAB dispersions ($DODAB^{NS}$) were prepared by hydrating crystals of the amphiphile in water at 57 °C for 20 min (above DODAB phase transition temperature) to the final concentration of 2 mM. After that, the sample was vortexed for 5 min and kept at room temperature for 3 h to stabilize. Dispersions so prepared were found by optical microscopy to be highly polydisperse, even exhibiting giant vesicles of diameters up to 10 μm (results not shown).

Sonication was performed with a tip sonifier (Virsonic 550-10A, Virtis Company Inc., Gardiner, NY, USA) with an 11.0 mm tip, at 30% of the total power, with the sample kept at ~60 °C. The sample was sonicated for 1 min several times, with 30 s interval between each sonication. Fig. 2 exhibits turbidity profiles of a typical DODAB sample (2 mM) after several cycles of sonication. In Fig. 2 inset (Absorbance at $\lambda = 250$ nm) it can be seen that the sample turbidity levels off around the 15th sonication procedure. Accordingly, sonicated DODAB dispersions ($DODAB^{S}$) were used after 15 sonication cycles and 1 h centrifugation at 15,000 rpm (at 24 °C) for the elimination of residual Ti. Measuring the sample turbidity, it could be detected that $DODAB^{S}$ dispersions presented some time evolution, reaching stability after 3 h incubation at room temperature. So, all experiments presented here were performed after that incubation time (samples were found to be stable for at least the next 24 h).

With optical microscopy it could be seen that the optical contrast of $DODAB^{S}$ dispersions was much lower than that of $DODAB^{NS}$ dispersions, compatible with the presence of much smaller aggregates. DSC profiles of $DODAB^{NS}$ and $DODAB^{S}$ dispersions, shown in Fig. 3, are similar to those in the literature [24–26]. $DODAB^{NS}$ presents a pre-transition at 35.5 °C (T_p) and a narrow, very cooperative main gel–fluid transition at 45 °C (T_m). In $DODAB^{S}$ dispersions, the shift of T_m to lower values, the double broad peak and the drop in the enthalpy of the transition (to approximately half the value of $DODAB^{NS}$) indicates the absence of large regions of DODAB in the gel phase, even at low temperatures. As discussed before [22], and shown here in Fig. 6, gel lipid regions can be detected below 35 °C by spin labels, but they should be small regions to give such a broad DSC peak. Hence, those results are in accord with the presence of DODAB bicelles in $DODAB^{S}$ dispersion.

2.3. AmB–DODAB dispersions preparation

AmB stock solution (500 μM) was prepared in dimethyl sulfoxide (DMSO):methanol (1:1). The antibiotic concentration was determined from its optical absorption spectra at 405 nm in methanol, based on the

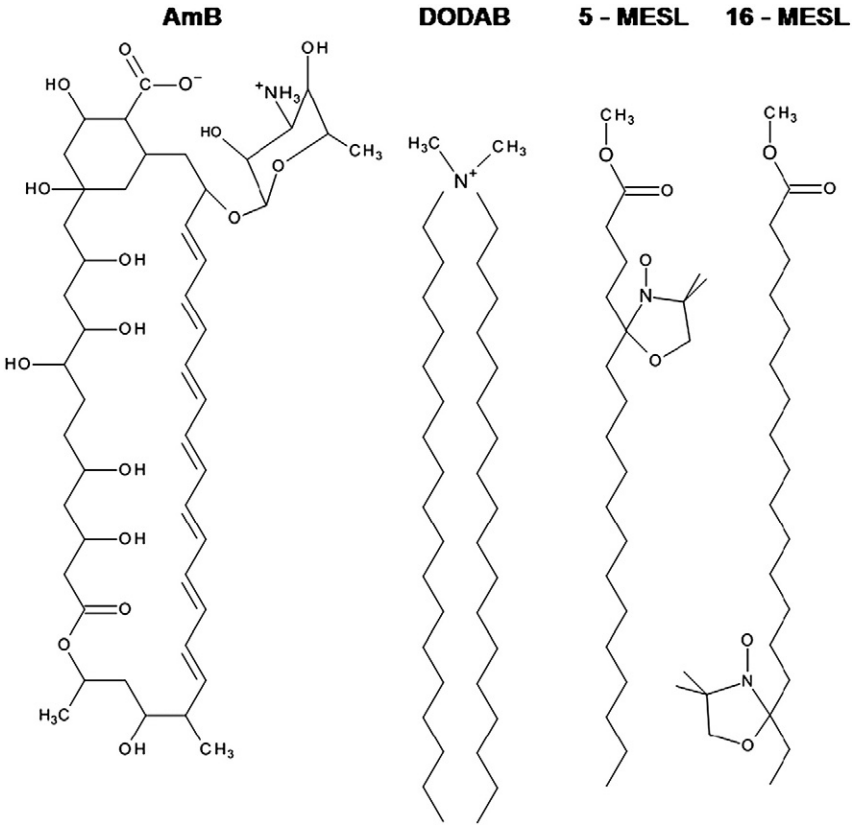

Fig. 1. Chemical structures of the antibiotic AmB, the amphiphile DODAB, and spin labels 5- and 16-MESL.

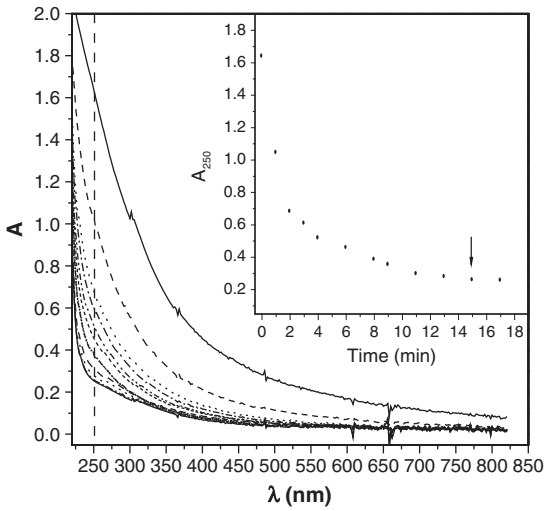

Fig. 2. Turbidity profiles (Absorbance versus λ) of DODAB dispersions after several sonication cycles. Dashed line shows the position (λ = 250 nm) where Absorbance was measured and plotted as a function of the sonication time (inset). Arrow in inset indicates the sonication time of DODAB^S dispersions used in the present work. Absorbance data were obtained at 23 °C. Optical pathway = 1 cm.

molar extinction coefficient ($\varepsilon = 1.56 \times 10^5\ M^{-1}\ cm^{-1}$) [27]. For the preparation of AmB in water, or AmB–DODAB dispersions, a small aliquot of the AmB stock solution was firstly dried under a stream of N_2 at the bottom of a tube, and then left under reduced pressure for at least 6 h for the evaporation of most of the organic solvents. After that, either water or prepared DODAB^{NS} or DODAB^S dispersions were added to the tube, vortexed for 5 min, incubated at room temperature for 6 h, and vortexed again before used. The sample turbidity was not much altered after the procedure described above. Several AmB–DODAB dispersions were prepared, corresponding to 0.4, 0.5, 0.6, 1.2 and 1.8 mol% of AmB relative to DODAB (2 mM).

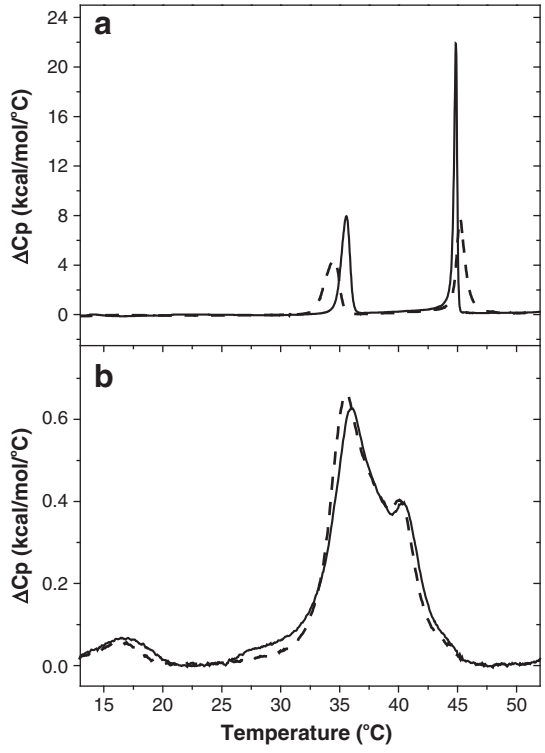

Fig. 3. Typical excess heat capacity (ΔCp) profiles of a) DODAB^{NS} in the absence (solid line) and presence (dashed line) of AmB (1.2 mol%) , and b) DODAB^S dispersions in the absence (solid line) and presence (dashed line) of AmB (1.2 mol%).

2.4. Extruded vesicle and AmB-extruded vesicle dispersions preparation

A lipid film of DPPC, DPPG or DODAB was formed from a chloroform solution, dried under a stream of N_2 and left under reduced pressure for a minimum of 2 h, to remove all traces of the organic solvent. Dispersions were prepared by the addition of 10 mM Hepes buffer pH 7.4 to the concentration of 2 mM, followed by vortexing for about 2 min at ca. 45 °C. After that, dispersions were extruded 31 times through a polycarbonate membrane at a temperature above the lipid phase transition (mini-extruder by Avanti Polar Lipids, 19 mm membranes with 100 nm pores, from Whatman plc, Maidstone, Kent, UK). Size distribution and stability were verified by Dynamic Light Scattering (DLS); (BI-200SM, Brookhaven Instruments Cop., Holtsville, NY, USA). The Z-average diameters were found to be (100 ± 5) nm, and the dispersions were found to be stable for at least 6 h. 1.2 mol% of AmB was added to the dispersions as described above for DODAB^{NS} or DODAB^S dispersions.

2.5. Optical microscopy

Dispersions were observed with a Ph2 63× objective in an inverted microscope Zeiss Axiovert 200 (Jena, Germany) equipped with a digital camera Zeiss AxioCam HSm (Jena, Germany). Sample was placed in a home-built observation chamber with a temperature-control jacket connected to a water circulating bath (images not shown here).

2.6. Differential scanning calorimetry

DSC traces were obtained by heating the samples from 5 to 60 °C, with a Microcalorimeter VP-DSC (MicroCal, Northampton, MA, USA), at 40 °C/h (identical traces were found at 20 °C/h). Baseline subtractions and peak integrals were performed using the MicroCal Origin software with the additional module for DSC data analysis provided by MicroCal, as described before [28].

2.7. Turbidity and absorption measurements

Optical absorption and turbidity (proportional to Absorbance measurements) were obtained with a HP UV–Vis 8452 A diode array spectrophotometer (Hewlett-Packard Co., Palo Alto, CA, USA). Temperature was controlled with a circulating water bath and measured inside the sample with a thermocouple. For AmB in the presence of lipid dispersion, the optical absorption spectrum of the antibiotic was obtained after the subtraction of the Absorbance due to pure lipid (see for instance, Fig. 2).

2.8. Balance between monomeric and aggregated AmB

The optical absorption spectrum of AmB is a fingerprint of its state of aggregation (see, for instance, [29–31]). In some organic solvents AmB is monomeric, presenting three narrow absorption bands (around 368, 388 and 412 nm), attributed to vibronic states (Fig. 4a). As shown in the inset of Fig. 4a, the positions of the three vibronic bands are solvent dependent. In water medium, at concentrations above 0.6 μM [32], the three bands nearly disappear, and a single blue-shifted broad band appears (between 320 and 344 nm), with no resolved vibrational structure (Fig. 4a). The ratio between the intensities of the monomer and aggregate peaks has been largely used in the literature to estimate the fraction of monomeric AmB present in the system (see, for instance, [33–35]). Here another parameter will be used, based on the ratio I_1/I_2 between the intensities of the two vibronic bands with longer wavelengths (I_1 and I_2 in Fig. 4a). Several arguments led us to choose this parameter, as discussed below. For the systems used here, the position of the peak due to AmB aggregate is not obvious. Actually, the position of this band has been reported to change from 320 to 350 nm, depending on the structure of the aggregate, and the medium where it is

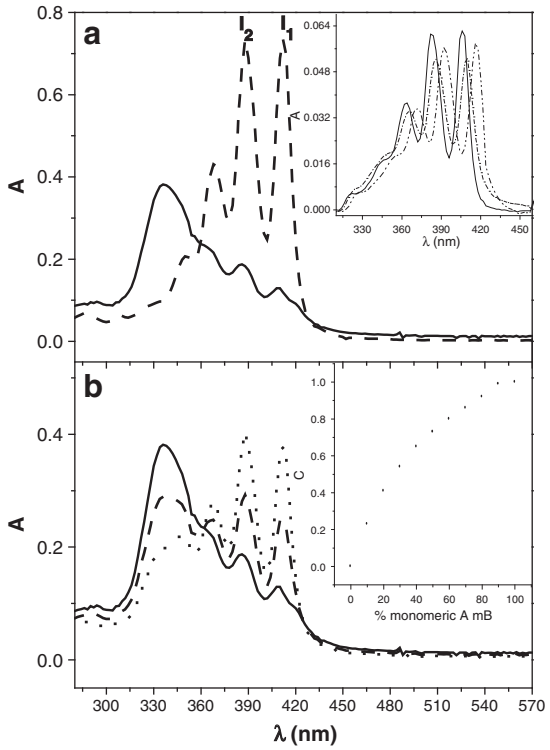

Fig. 4. a) Optical spectra of 24 μM AmB in DMSO/Methanol (1/1) (dashed line) and in water (solid line) media. The inset displays 0.4 μM AmB in methanol (solid line), water (dashed line) and DMSO (dotted line). b) Composite spectra obtained from the addition of different percentages of the optical spectra of monomeric and aggregated AmB: 0% monomeric (solid line), 30% monomeric (dashed line) and 60% monomeric (dotted line). The inset shows the variation of the C parameter (Section 2.8), measured on the composite spectra, as a function of the percentage of monomeric AmB. T = 23 °C. Optical path = 0.2 cm. For the inset in a), optical path = 1.0 cm.

formed [30–32,36]. Besides, in AmB-lipid systems it would be possible to have the presence of different kinds of aggregates, for instance, aggregated AmB in water and bound to the lipid membrane. Moreover, the optical intensity around 320 nm is more distorted by light scattering than the intensity at longer wavelengths. Light scattering is due to the presence of both amphiphile and AmB aggregates.

The position of the vibronic bands can change for different solvents (see inset in Fig. 4a), but the ratio $(I_1/I_2)_{Mon}$ was found to be 1.01 ± 0.01 considering 8 different monomeric AmB samples. For aggregated AmB in water medium, $(I_1/I_2)_{Agg}$ was found to be 0.58 ± 0.05 (from 10 samples). Hence, considering that AmB is mostly aggregated in water medium, the balance between AmB monomers and aggregates can be estimated by the ratio (I_1/I_2), which is close to 1.0 for monomeric AmB, and decreases in the presence of AmB aggregates. Accordingly, an experimental quantitative parameter, which varies from 1 (AmB monomeric) to 0 (AmB in water, mostly aggregated), was used for the evaluation of the balance between AmB monomers and aggregates,

$$C = \frac{(I_1/I_2) - (I_1/I_2)_{Agg}}{(I_1/I_2)_{Mon} - (I_1/I_2)_{Agg}}$$

where (I_1/I_2) is the ratio measured at the optical spectrum of the system to be analyzed. To test this parameter, optical spectra of aggregated and monomeric AmB (Fig. 4a) were added at different proportions (Fig. 4b), and the C parameter was measured on the composite spectrum. Fig. 4b evidences the sensitivity of the C parameter to the balance between monomeric and aggregated AmB. This parameter is certainly just an indication of the fractions of monomeric and aggregated AmB, as it assumes that AmB is totally aggregated in water and the optical spectrum of aggregated AmB does not change with AmB concentration. (Hence, the optical spectrum of AmB in water is our reference for "aggregated AmB").

2.9. ESR spectroscopy

ESR measurements at X-band were performed with a Bruker EMX spectrometer. Field-modulation amplitude of 1 G and microwave power of 5 mW was used. The temperature was controlled to about 0.2 °C with a Bruker BVT-2000 variable temperature device, and monitored with a Fluke 51 K/J thermometer with a probe placed just above the cavity. The magnetic field was measured with a Bruker ER 035 NMR Gausmeter. All ESR data shown are means of the results of at least three experiments, and the uncertainties are the standard deviations. Spin labeled samples were prepared as described before [22].

2.10. ESR spectra analysis

For the ESR spectra simulations, the computer program NLLS developed by Freed and coworkers [37,38] was used. The parameters were obtained from nonlinear least squares fitting of the experimental ESR signal based on the stochastic Liouville equation [39]. The dynamics of the spin label is characterized by a rotational correlation time (τ), calculated from the principal components of the axially symmetric rotational diffusion tensor, $R_{//}$ and $R_{\perp}$. For 5- and 16-MESL they represent the rotational rates of the nitroxide moiety around axes parallel and perpendicular to the hydrocarbon chain, respectively. For the simulations, we found adequate to assume the axially symmetric rotational diffusion tensor with $R_{//}/R_{\perp} = 10$. The average rotational diffusion rate is defined as $\overline{R} = \sqrt[3]{R_{\perp}^2 R_{//}}$ and $\tau = (6\overline{R})^{-1}$ [38,39]. The local microscopic order of the spin label in the lipid bilayer is characterized by the order parameter, S_0, calculated from the best parameters obtained from the first terms of the expansion of the ordering potential in generalized spherical harmonics [37]. From the hyperfine tensor components A_{xx}, A_{yy} and A_{zz}, an isotropic hyperfine splitting was calculated ($a_o = (A_{xx} + A_{yy} + A_{zz})/3$). For simplicity, A_{zz} was varied, while A_{xx} and A_{yy} were kept constant at 5.319 and 5.300 G, respectively. The principal g-values were kept at $g_{xx} = 2.0089$, $g_{yy} = 2.0058$, $g_{zz} = 2.0022$.

For temperatures above DODAB gel–fluid transition, for 16-MESL in fluid $DODAB^S$ and $DODAB^{NS}$ bilayers, the ESR spectra were analyzed according to the methodology developed by Bales [40]. By the motional narrowing theory [41], rotational correlation time for isotropic motion can be calculated from the peak-to-peak width of the ESR Lorentzian lines [42,43]:

$$\Delta H_L(m) = A + Bm + Cm^2$$

Where m is the mth component of the nitrogen nuclear spin, A is the Lorentzian linewidth of the central line, $\Delta H_L(0)$, and B and C are

$$B = \frac{1}{2}\Delta H_L(0)\left(\frac{\Delta H_L(+1)}{\Delta H_L(0)} - \frac{\Delta H_L(-1)}{\Delta H_L(0)}\right)$$

$$C = \frac{1}{2}\Delta H_L(0)\left(\frac{\Delta H_L(+1)}{\Delta H_L(0)} + \frac{\Delta H_L(-1)}{\Delta H_L(0)} - 2\right)$$

The correlation time for doxyl labels is either $\tau_B = -1.22\ B$ or $\tau_C = 1.19\ C$, ($\tau_B = \tau_C$ for isotropic movement). Lorentzian linewidths are calculated using a computer program, which performs nonlinear least-square fitting of the experimental ESR spectrum using a model of a Lorentzian–Gaussian function for corrections for non-resolved hyperfine splitting [40,44]. The isotropic hyperfine splitting (a_0) is directly calculated from the spectrum fitting.

Another ESR parameter used here, the maximum hyperfine splitting, A_{max}, directly measured on the ESR spectrum (see Fig. 6, top spectra), increases with the label microenvironment viscosity or packing [39].

3. Results and discussion

3.1. Optical absorption

Fig. 5a shows the optical absorption spectra of AmB in DODAB^S dispersion, at different AmB–DODAB molar ratios, from 0.4 to 1.8 mol% (AmB–DODAB dispersions were prepared as described in Sections 2.2 and 2.3). Qualitatively comparing Fig. 5a and Fig. 4a, it could be concluded that AmB is mostly monomeric, as the optical spectra of the different dispersions are similar to that obtained for the AmB monomer. However, it is possible to make a better analysis, calculating the C parameter as described in Section 2.8. The inset in Fig. 5a shows that up to around 1.2 mol% of AmB–DODAB the antibiotic is mostly monomeric in DODAB^S dispersions, as C~1.0. Hence, most of the experiments discussed below were performed at that AmB–DODAB molar percentage. Results shown in Fig. 5a were obtained at 23 °C, but rather similar results were obtained at 50 °C, with DODAB^S.

It is interesting to point out that for linear polyenes the position of the vibronic bands is related to the refractive index of the medium. It has been shown that the absorption transition of these chromophores shifts mainly in response to the polarizability of the environment (proportional to the medium refractive index) and not to the solvent polarity (proportional to the medium dielectric constant), due to the small electric dipole moment of the polyene and its large electric transition dipole [45]. For instance, for the longer wavelength band, λ = 405, 409 and 417 nm, in methanol (n = 1.3284), water (n = 1.3330) and DMSO (n = 1.4793), respectively (inset in Fig. 4a). The position of this band in AmB–DODAB^S systems (λ = 413 nm, Fig. 5a), indicates that the polyenic moiety of AmB is not fully exposed to water, but embedded in a microenvironment with optical characteristics (refractive index) between water and DMSO (in DODAB^S aggregate).

A small fraction of monomeric AmB could be detected in the presence of DODAB^{NS}, following the incubation procedure here described (Section 2.3), though a detailed analysis of the optical spectra is difficult, due to the high sample turbidity (see Fig. 2). Fig. 5b shows the optical Absorbance spectra of AmB–DODAB^{NS} (1.2 mol%) dispersions, after the subtraction of the turbidity background. AmB is clearly less aggregated at 23 °C, in the presence of gel DODAB bilayers (C = 0.66) than at 50 °C, in the presence of fluid membrane (C = 0.47). This is not the focus of the present work, and needs further investigation, as it is not obvious that this observed difference is related to the phase of the lipid, as it is known that AmB self-aggregation properties are strongly temperature dependent [31]. The position of the longer wavelength vibronic band (λ ~ 414 nm, Fig. 5b) indicates that AmB is inserted into the bilayer.

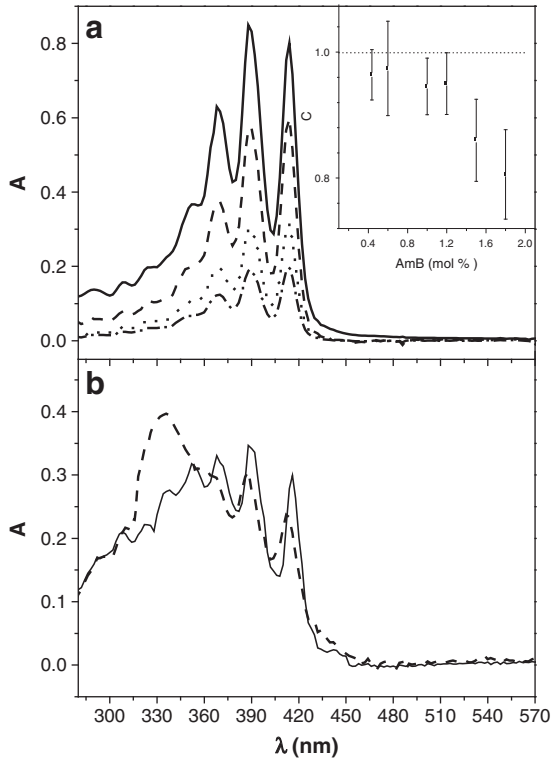

Fig. 5. a) Optical spectra of different AmB–DODAB^S dispersions: 0.4 (dash-dot line), 0.60 (dotted line), 1.2 (dashed line) and 1.8 mol% (solid line). The inset shows the C parameter (Section 2.8) for the different AmB–DODAB^S molar ratios (data are average values of at least 6 experiments, with the corresponding standard deviations). T = 23 °C. b) Optical spectra of AB–DODAB^{NS} dispersions (1.2 mol%), at gel (solid line, T = 23 °C) and fluid (dashed line, T = 50 °C) phases. Optical path = 0.2 cm.

3.2. DSC

Supporting the data obtained with optical absorption, where monomeric AmB could be detected in the presence of DODAB^{NS} dispersion, indicating some AmB–DODAB interaction, the DSC trace of DODAB^{NS} in the presence of AmB (1.2 mol%, AmB–DODAB) was found to be somehow altered. Fig. 3a shows typical DSC traces, indicating that the presence of AmB decreases DODAB bilayer pre-transition temperature, increases T_m, and slightly decreases the enthalpy of the transitions: pre-transition ΔH changes from 5 ± 2 to 3 ± 2 kcal/mol, and for the main transition, from 10.8 ± 0.6 to 10.1 ± 0.4 kcal/mol, in the presence of 1.2 mol% AmB. The modest impact of AmB on DODAB^{NS} thermal properties should be related to the relative small amount of bound molecules, and/or to their interaction at the bilayer surface.

As mentioned before, the thermal events monitored with DODAB^S aggregates are much broader and less intense (ΔH ~ 5 ± 1 kcal/mol) than those with DODAB^{NS}. It is interesting to observe that AmB does not alter the DODAB^S DSC profile (Fig. 3b). This suggests that AmB does not interact at regions where DODAB is in the gel phase, as those would be the regions responsible for the monitored thermal events. This point will be further discussed below.

3.3. ESR

When 5 and 16-MESL spin labels are incorporated in DODAB^{NS} vesicles below T_m (15 and 30 °C), their ESR spectra are typical of spin labels in a gel phase bilayer ([22]; Fig. 6, top spectra). As 5-MESL monitors a shallower position in the membrane, around the 5th carbon atom of the acyl chain, its ESR spectrum is more anisotropic (larger A_{max} parameter, indicated in Fig. 6, top spectra) than that of 16-MESL, which monitors the bilayer core, showing that the movement of 5-MESL is more restricted than that of 16-MESL. This is due to the well-known flexibility gradient towards the bilayer midpoint [46]. Though AmB was found to interact with DODAB^{NS} vesicles by optical spectroscopy (Fig. 5b) and DSC (Fig. 3), no significant change on 5- and 16-MESL ESR spectra could be detected at the concentrations used here (up to 1.8 mol% AmB). This is possibly due to the small amount of monomeric AmB bound to the lipid vesicle, according to Fig. 5b. On the other hand, even if the total amount of AmB would bind, the effect could be negligible, as spin labels are usually not sensitive to small amounts of bound ligand.

As discussed before [22], opposite to DODAB^{NS}, DODAB^S dispersions, at the same temperatures, clearly indicate the coexistence of gel and fluid domains (Fig. 6, middle spectra, with dashed lines indicating the position of the outer features of the gel phase signal). That coexistence of gel and fluid lipids indicate the presence of DODAB bicelles, with gel lipids corresponding to the bilayer region, and fluid lipids to the edges of

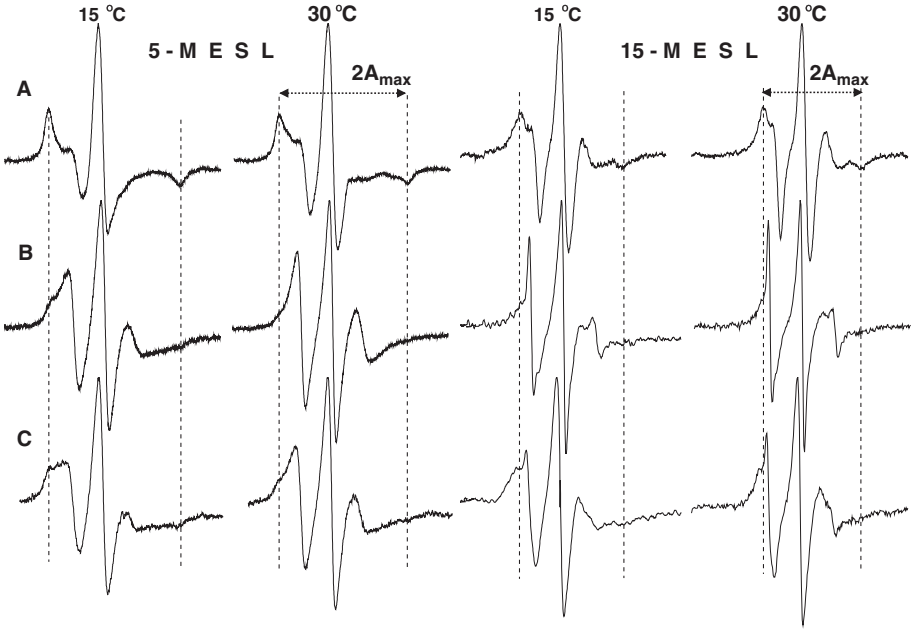

Fig. 6. ESR spectra of spin labels (5-MESL and 16-MESL) incorporated in DODAB^{NS} dispersions (A, top spectra), and DODAB^{S} dispersions without (B, middle spectra) and with 1.2 mol% of AB (C, bottom spectra), at 15 °C and 30 °C. Dashed lines indicate the positions of the outer features of the gel phase spectrum (outer hyperfine splitting, $2A_{max}$). Total spectra width 100 G.

the bicelle [22]. According to the strong affinity of monomeric AmB to DODAB^{S} bicelles (Fig. 5a), AmB–DODAB^{S} interaction (1.2 mol%) clearly changes the ESR spectra of both 5- and 16-MESL (Fig. 6, bottom traces), even at that relative small concentration (relative AmB–DODAB concentration will be further discussed below).

The ESR spectra shown in Fig. 6, obtained with spin labels incorporated in DODAB^{NS} and DODAB^{S} aggregates bellow T_m, were analyzed by the simulation procedure developed by Freed and coworkers [37,38] (Section 2.10). 5- and 16-MESL incorporated in DODAB^{NS} vesicles at 30 °C could be well simulated as a single ESR signal, corresponding to a gel bilayer (not shown). As expected, 5- and 16-MESL in DODAB^{S} aggregates at 15 and 30 °C could not be simulated as single ESR spectra, and required two components for a satisfactory fit. That is in accord with the above discussion, concerning the presence of gel and fluid lipids in DODAB bicelles below T_m. Hence, the decomposition of the ESR signal into two components allowed the independent analysis of the effect of AmB on the bilayer fragment of the bicelle (gel lipids), and on its edges (fluid lipids).

Fig. 7 shows the simulation of the spectrum of 16-MESL in DODAB^{S} dispersions as a composite spectrum (at the top, the solid line is the experimental spectrum and the dashed line is the simulation), constituted by an ESR signal typical of a gel lipid membrane (gel-component in Fig. 7, second spectrum from the top), and another more isotropic signal, typical of the label in a rather fluid micro-environment (fluid-component in Fig. 7, third spectrum from the top).[1] That confirms the previous qualitative analysis [22], which indicated the coexistence of two different environments in DODAB^{S} aggregates below T_m. Similar analysis was performed in the presence of AmB, with 16-MESL incorporated in AmB–DODAB^{S} dispersions, at different AmB–DODAB molar ratios. Fig. 7 (4th spectrum from the top) shows the experimental spectrum obtained with 16-MESL in 1.2 mol% dispersion of AmB–DODAB^{S} (solid line) and the best fit simulation (dashed line). The two components obtained from the simulation are the last two bottom signals. All simulated spectra were in very good agreement with the experimental ones.

[1] Similar simulations could be performed with 5-MESL ESR spectra. However, due to the characteristics of the spectra, the simulation parameters were not as unambiguously defined as those obtained with 16-MESL spectra, and will not be discussed here.

It was interesting to find that the fractions of the gel (0.85) and fluid (0.15) components were not altered by the presence of AmB, suggesting that DODAB bicelles were not significantly modified (for instance, by fusion or any rearrangement of the amphiphiles). However, due to the unknown partition of the probe molecule into DODAB fluid and gel regions, it is not possible to infer that the bicelle is composed by 85% and 15% lipids in the gel bilayer and fluid edges, respectively. For instance, NMR data indicated that the DODAB bicelle fluid edges were composed by 50% of the amphiphile population [24], though a somewhat different procedure for preparing the DODAB^{S} dispersion was used.

Spectral changes observed in the presence of AmB were found to be mostly due to alterations in the shape of the fluid-component signal, according to the following discussion. ESR signals of the two components were analyzed considering the best fit values for the rotational correlation time, τ, order parameter, S_o, and isotropic hyperfine splitting, a_o (Section 2.10). Fig. 8 (open symbols) shows that AmB rigidifies the fluid domains of DODAB^{S} aggregates, as the presence of the antibiotic increases the spin label rotational correlation time and increases the order parameter of the edges region. Concomitantly, AmB slightly decreases the polarity of those fluid domains in DODAB^{S} bicelles, as the presence of the antibiotic causes a small decrease in the isotropic hyperfine splitting [47]. Considering the structure of AmB molecule (Fig. 1), with the hydrophobic conjugated double-bond chain on one side of the ring, and the hydrophilic –OH groups on the other, it is reasonable to think that the molecule would stay at the lipid aggregate surface, with the polyene chain embedded into the aggregate, indicated by the position of the vibronic bands, but with the hydrophilic –OH groups and the sugar moiety at the water interface. It is noteworthy that structural modifications caused by AmB on the amphiphile aggregate propagates down to the 16th C-atom of the label acyl chain (modifies 16-MESL ESR spectrum), even with the antibiotic probably located at the bicelle surface. Considering that the mobility of a C–C moiety at the bilayer core is dependent on the mobility of the whole chain, it has been suggested [48] that if the interacting molecule restrains the freedom of the first two or three carbons, without separating the hydrocarbon chains, the rigidifying effect could propagate till the end of the hydrocarbon chain, as it reduces the overall chain configuration space.

Fig. 8 indicates that 1.2 mol% AmB is somehow a limiting AmB concentration. That is interesting because above this AmB–DODAB

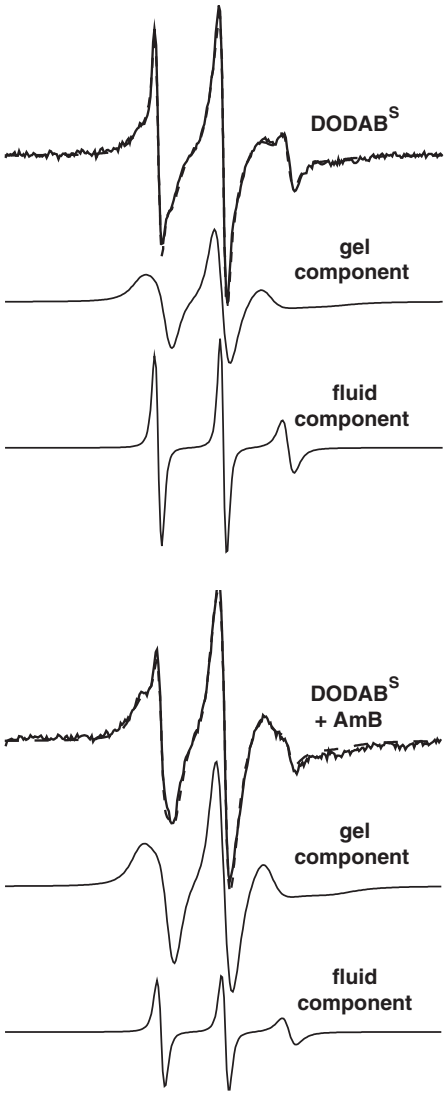

Fig. 7. ESR spectra of 16-MESL incorporated in DODAB^S and DODAB^S with 1.2 mol% of AB. From the top, solid lines in the first and the third ESR spectra correspond to the experimental spectra of DODAB^S and AmB–DODAB^S, respectively, and dashed lines to the best fit simulations. The ESR signals below the first and the third ESR spectra are the two components obtained from spectral simulation. T = 30 °C.

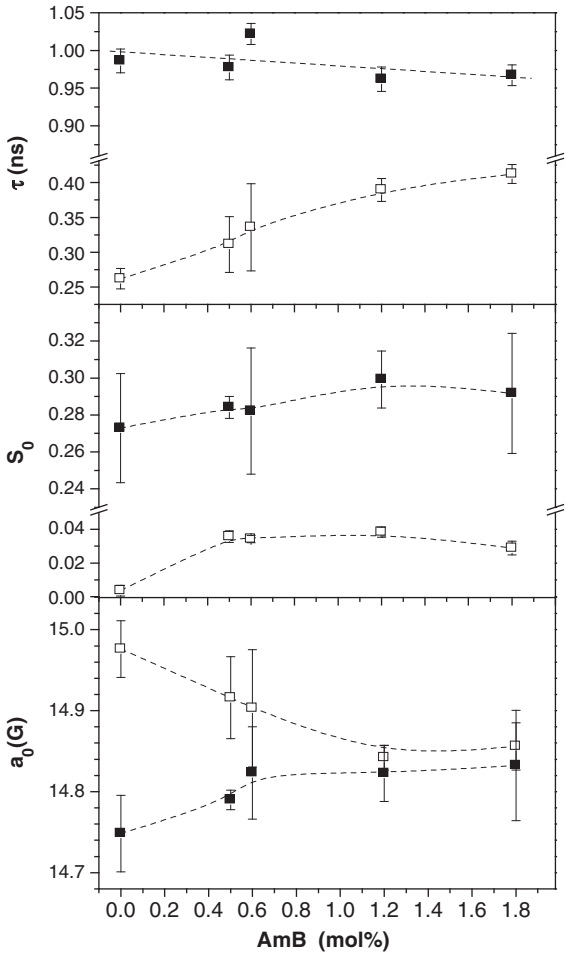

Fig. 8. For the fluid-component (open symbols) and the gel-component (closed symbols) of 16-MESL in DODAB^S aggregates, plots of the best fit values of the rotational correlation time, τ, the order parameter, S_o, and the isotropic hyperfine splitting, a_o, as a function of AmB–DODAB molar ratio.

concentration AmB aggregates were found to coexist with monomeric AmB in DODAB bicelle (see inset in Fig. 5a, and related discussion in the text). Putting together the optical absorption data (inset in Fig. 5a) and the ESR data (Fig. 8, open symbols), it can be concluded that, for the DODAB and AmB concentrations used here, it is mostly AmB monomers that are interacting with the amphiphile bicelle, and AmB self-aggregates are formed in solution for concentrations above ~1.2 mol% AmB.

A possible schematic representation of the interaction of monomeric AmB with DODAB^S bicelle is shown in Fig. 9, where it is considered that monomeric AmB is better solubilized in DODAB bicelle edges as compared to bicelle gel bilayers. Amphiphile and antibiotic molecules are drawn to scale, and the relative proportion between AmB and DODAB molecules in the bicelle, 1.2/100, is also roughly considered. It is important to have in mind that if AmB interacts preferentially at the fluid edges of the bicelle, the ratio 1.2/100 of AmB/DODAB molecules would be higher at that region. Hence, if only 15% of DODAB molecules are along the bicelle border (considering equal partition of spin labels in gel and fluid domains, as discussed above), the ratio would be around 8/100 of AmB/DODAB molecules, alternatively, it would be 2.4/100, if the NMR data is considered, and it is assumed that 50% of the amphiphile are in the edges [24].

As expected, for the gel-component of 16-MESL incorporated in DODAB^S bicelles, which corresponds to the probe at the gel bilayer portion of the bicelle, the rotational correlation time and the order parameter are larger and the hyperfine splitting is smaller, as compared to the parameters obtained for the fluid-component (comparing data corresponding to AmB = 0 in Fig. 8, open and closed symbols). Interestingly, the presence of AmB only slightly affects the best fitting parameters (Fig. 8, closed symbols), indicating that AmB is

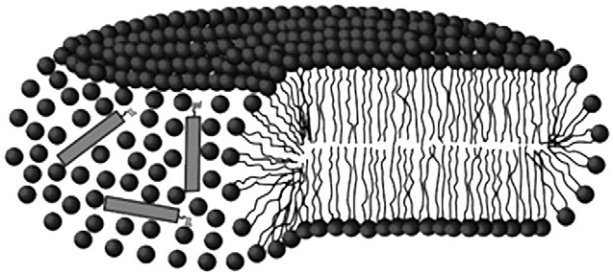

Fig. 9. Schematic representation of AmB bound to a DODAB bicelle. AmB is represented as a rigid rectangle with the sugar moiety.

mostly bound at the edges of the DODAB^S bicelle, disturbing the fluid-component ESR signal, as discussed above (Fig. 8, open symbols).

For higher temperatures, above DODAB T_m, 16-MESL in both DODAB^{NS} and DODAB^S dispersions yielded ESR spectra typical of the spin label in fluid bilayers (Fig. 10). That is, it was not possible to decompose the ESR signal of 16-MESL (or 5-MESL) in DODAB^S bicelles into two components (corresponding to spin labels in the bilayer and in the bicelle edge), possibly due to the similarity of the two signals and/or the quick exchange of spin labels between the two domains (in the ESR time scale, ns). 16-MESL ESR spectra are typical of the motional narrowing regime, and the spectra can be well analyzed by the fitting of each hyperfine line by a Voigt function, what allows the calculation of the spin label isotropic rotational correlation time and the isotropic hyperfine splitting (Section 2.10). The two correlation times were calculated, τ_B and τ_C, and found to be very similar, indicating that the nitroxide moiety of 16-MESL is located in a quasi-isotropic microenvironment [43], so only τ_C is presented in Fig. 11a. AmB slightly increases the bicelle fluidity in DODAB^S dispersions, decreasing the probe rotational correlation time from 0.32 ns to 0.28 ns. Though the effect of AmB is opposite of that found at lower temperatures (Fig. 8), 1.2 mol% of AmB is also the limiting AmB concentration for fluid DODAB^S dispersions. The opposite effects AmB causes in fluid and gel bicelles, does not seem to be due to the possible incorporation of AmB in the bilayer part of fluid bicelles, as AmB in DODAB^{NS} fluid bilayers was found to slightly increase τ_C (Fig. 11a). Similar to the effect found at low temperatures (Fig. 8), AmB decreases the bilayer polarity of DODAB bicelles in DODAB^S dispersions (decreases a_o), presenting the same effect on DODAB^{NS} fluid vesicles (Fig. 11b). Hence, spin labels indicate that AmB binds to fluid DODAB bicelles and vesicles. However, this small fluidizing effect of AmB on fluid DODAB bicelles remains to be better understood.

3.4. Comparing AmB binding to DODAB, DPPC and DPPG

To further characterize the binding of AmB to DODAB aggregates, 1.2 mol% of AmB was incubated with extruded vesicles of DODAB, DPPG and DPPC. As mentioned in Section 2.4, the three amphiphiles form LUV vesicles of similar radii, so the vesicle bilayers have similar curvature. It was found that AmB is better adsorbed in the cationic DODAB bilayer ($C = 0.83 \pm 0.01$) than in the anionic DPPG bilayer ($C = 0.71 \pm 0.02$) or in the zwitterionic DPPC ($C = 0.63 \pm 0.01$). It could be speculated that the small DODAB polar headgroup facilitates the insertion of the AmB polyene chain into the hydrophobic portion of the bilayer. Comparing AmB binding to DODAB vesicles (1.2 mol% of AmB relative to the amphiphile) before and after extrusion, and DODAB bicelles, after sonication, it is clear that monomeric AmB adsorbs preferentially onto bicelles ($C \sim 1$, Fig. 5a), followed by DODAB extruded vesicles ($C \sim 0.83$), and DODAB^{NS} vesicles ($C \sim 0.66$, Fig. 5b).

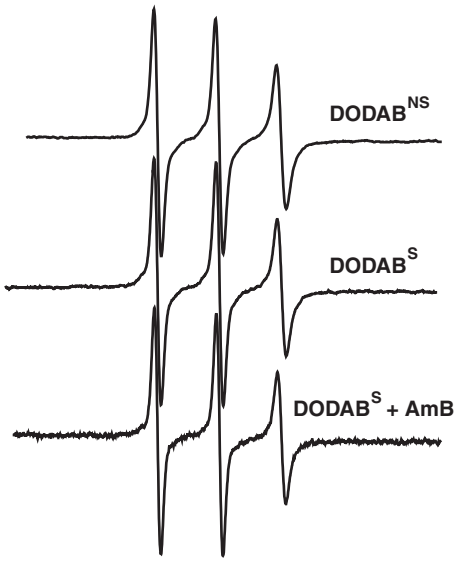

Fig. 10. ESR spectra of 16-MESL incorporated in DODAB^{NS} dispersion (top spectra), and DODAB^S dispersion without (middle spectra) and with 1.2 mol% of AmB (bottom spectra), at 50 °C. Total spectra width 100 G.

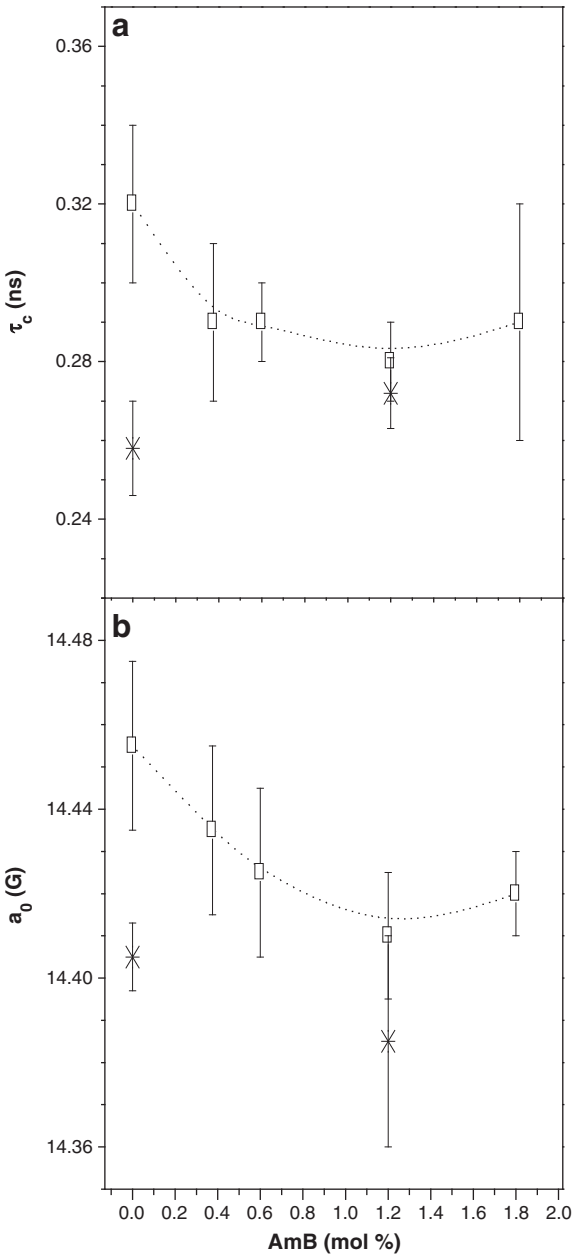

Fig. 11. (a) Rotational correlation time (τ_c) and (b) isotropic hyperfine splitting (a_o) calculated from the ESR spectra of 16-MESL in AmB–DODAB^S (□) and DODAB^{NS} (*) dispersions as a function of AmB–DODAB molar ratio. T = 50 °C.

4. Conclusions

For concentrations up to 1.2 mol% of AmB relative to DODAB ([DODAB] = 2 mM, [AmB] = 24 μM), AmB was found to be mostly monomeric, adsorbed onto the DODAB^S bicelle. For the same AmB–DODAB relative concentration, in the presence of DODAB^{NS} vesicles and DODAB extruded vesicles, self-aggregated AmB in solution coexisting with monomeric adsorbed antibiotic could be detected. As discussed

before [49], monomeric AmB binds preferentially to more curved bilayers, namely to smaller extruded vesicles as compared with large $DODAB^{NS}$ vesicles. Considering vesicles of the same curvature, it was found that monomeric AmB exhibits higher affinity for DODAB than for the natural lipids DPPC and DPPG, possibly due to the small DODAB polar headgroup. To estimate the balance between monomeric and self-aggregated AmB, a parameter was defined here (C), based on the ratio between the intensities of the two vibronic bands with longer wavelengths.

Using the fact that spin labels can separately monitor the two different domains in a gel bicelle, namely the gel bilayer and the fluid borders, with theoretical simulations of the ESR spectra of spin labels incorporated in DODAB bicelles below 40 °C, it could be proved that monomeric AmB binds preferentially to lipids located at the edges of $DODAB^{S}$ bicelles, rigidifying them, and decreasing the polarity of the region. That special binding of monomeric AmB along the borders of bicelles, where the lipids are highly disorganized, could be used in the preparation of other carriers for the antibiotic, including mixtures of natural lipids which are known to form bicelles [50].

Acknowledgments

This work was supported by USP, FAPESP and CNPq (MTL research fellowship). We are grateful to Dr. A. M. Carmona-Ribeiro for initial discussions, to Dr. K. A. Riske for helping with the optical microscope experiments, and to T. S. Ribeiro for helping with the experiments with extruded vesicles.

References

[1] S. Hartsel, J. Bolard, Amphotericin B: new life for an old drug, Trends Pharmacol. Sci. 17 (1996) 445–449.
[2] D.W. Denning, W.W. Hope, Therapy for fungal diseases: opportunities and priorities, Trends Microbiol. 18 (2010) 195–204.
[3] H.A. Gallis, R.H. Drew, W.W. Pickard, Amphotericin-B — 30 years of clinical-experience, Rev. Infect. Dis. 12 (1990) 308–329.
[4] J. Bolard, How do the polyene macrolide antibiotics affect the cellular membrane-properties, Biochim. Biophys. Acta. 864 (1986) 257–304.
[5] G. Fujii, J.E. Chang, T. Coley, B. Steere, The formation of amphotericin B ion channels in lipid bilayers, Biochemistry-US 36 (1997) 4959–4968.
[6] B.E. Cohen, Amphotericin B membrane action: role for two types of ion channels in eliciting cell survival and lethal effects, J. Membr. Biol. 238 (2010) 1–20.
[7] M.T. Lamy-Freund, V.F.N. Ferreira, S. Schreier, Mechanism of inactivation of the polyene antibiotic amphotericin-B — evidence for radical formation in the process of autooxidation, J. Antibiot. 38 (1985) 753–757.
[8] M. Sokolanderson, J.E. Sligh, S. Elberg, J. Brajtburg, G.S. Kobayashi, G. Medoff, Role of cell defense against oxidative damage in the resistance of candida-albicans to the killing effect of amphotericin-B, Antimicrob. Agents. Chemother. 32 (1988) 702–705.
[9] F. Sangalli-Leite, L. Scorzoni, A.C. Mesa-Arango, C. Casas, E. Herrero, M.J.S.M. Gianinni, J.L. Rodriguez-Tudela, M. Cuenca-Estrella, O. Zaragoza, Amphotericin B mediates killing in *Cryptococcus neoformans* through the induction of a strong oxidative burst, Microb. Infect. 13 (2011) 457–467.
[10] J. Brajtburg, J. Bolard, Carrier effects on biological activity of amphotericin B, Clin. Microbiol. Rev. 9 (1996) 512.
[11] J.J. Torrado, R. Espada, M.P. Ballesteros, S. Torrado-Santiago, Amphotericin B formulations and drug targeting, J. Pharm. Sci. 97 (2008) 2405–2425.
[12] J. Bolard, P. Legrand, F. Heitz, B. Cybulska, One-sided action of amphotericin-B on cholesterol-containing membranes is determined by its self-association in the medium, Biochemistry-US 30 (1991) 5707–5715.
[13] J. Barwicz, P. Tancrede, The effect of aggregation state of amphotericin-B on its interactions with cholesterol- or ergosterol-containing phosphatidylcholine monolayers, Chem. Phys. Lipids. 85 (1997) 145–155.
[14] M.T. Lamy-Freund, V.F.N. Ferreira, S. Schreier, Polydispersity of aggregates formed by the polyene antibiotic amphotericin-B and deoxycholate — a spin label study, Biochim. Biophys. Acta. 981 (1989) 207–212.
[15] M.T. Lamy-Freund, S. Schreier, R.M. Peitzsch, W.F. Reed, Characterization and time-dependence of amphotericin-B: deoxycholate aggregation by quasielastic light-scattering, J. Pharm. Sci. 80 (1991) 262–266.
[16] J. Barwicz, S. Christian, I. Gruda, Effects of the aggregation state of amphotericin-B on its toxicity to mice, Antimicrob. Agents. Chemother. 36 (1992) 2310–2315.
[17] P. Legrand, E.A. Romero, B.E. Cohen, J. Bolard, Effects of aggregation and solvent on the toxicity of amphotericin-B to human erythrocytes, Antimicrob. Agents. Chemother. 36 (1992) 2518–2522.
[18] D.B. Vieira, A.M. Carmona-Ribeiro, Synthetic bilayer fragments for solubilization of amphotericin B, J. Colloid. Interf. Sci. 244 (2001) 427–431.
[19] N. Lincopan, E.M. Mamizuka, A.M. Carmona-Ribeiro, Low nephrotoxicity of an effective amphotericin B formulation with cationic bilayer fragments, J. Antimicrob. Chemother. 55 (2005) 727–734.
[20] M.J. Blandamer, B. Briggs, P.M. Cullis, P. Last, J.B.F.N. Engberts, A. Kacperska, Effects of added urea and alkylureas on gel to liquid–crystal transitions in DOAB vesicles, J. Therm. Anal. Calorim. 55 (1999) 29–35.
[21] M. Andersson, L. Hammarstrom, K. Edwards, Effect of bilayer phase-transitions on vesicle structure and its influence on the kinetics of viologen reduction, J. Phys. Chem. 99 (1995) 14531–14538.
[22] C.R. Benatti, E. Feitosa, R.M. Fernandez, M.T. Lamy-Freund, Structural and thermal characterization of dioctadecyldimethylammonium bromide dispersions by spin labels, Chem. Phys. Lipids. 111 (2001) 93–104.
[23] R.B. Pansu, B. Arrio, J. Roncin, J. Faure, Vesicles versus membrane-fragments in DODAC suspensions, J. Phys. Chem. 94 (1990) 796–801.
[24] J. Cocquyt, U. Olsson, G. Olofsson, P. Van der Meeren, Temperature quenched DODAB dispersions: fluid and solid state coexistence and complex formation with oppositely charged surfactant, Langmuir 20 (2004) 3906–3912.
[25] R.O. Brito, E.F. Marques, Neat DODAB vesicles: effect of sonication time on the phase transition thermodynamic parameters and its relation with incomplete chain freezing, Chem. Phys. Lipids. 137 (2005) 18–28.
[26] C.R. Benatti, M.J. Tiera, E. Feitosa, G. Olofsson, Phase behavior of synthetic amphiphile vesicles investigated by calorimetry and fluorescence methods, Thermochim. Acta 328 (1999) 137–142.
[27] J. Milhaud, B. Michels, Binding of nystatin and amphotericin B with sterol-free L-dilauroylphosphatidylcholine bilayers resulting in the formation of dichroic lipid superstructures, Chem. Phys. Lipids. 101 (1999) 223–235.
[28] K.A. Riske, R.P. Barroso, C.C. Vequi-Suplicy, R. Germano, V.B. Henriques, M.T. Lamy, Lipid bilayer pre-transition as the beginning of the melting process, BBA-Biomembranes 1788 (2009) 954–963.
[29] C. Ernst, J. Grange, H. Rinnert, G. Dupont, Structure of amphotericin-B aggregates as revealed by UVand CD spectroscopies, Biopolymers 20 (1981) 1575–1588.
[30] J. Barwicz, W.I. Gruszecki, I. Gruda, Spontaneous organization of amphotericin-B in aqueous-medium, J. Colloid. Interf. Sci. 158 (1993) 71–76.
[31] F. Gaboriau, M. Cheron, L. Leroy, J. Bolard, Physico-chemical properties of the heat-induced 'superaggregates' of amphotericin B, Biophys. Chem. 66 (1997) 1–12.
[32] M.T. Grijalba, M. Cheron, E. Borowski, J. Bolard, S. Schreier, Modulation of polyene antibiotics self-association by ions from the hofmeister series, BBA-Gen. Subjects 1760 (2006) 973–979.
[33] G. Strauss, The interaction of amphotericin-B with lipid bilayer vesicles — determination of binding constants by absorption and fluorescence spectroscopy, Can. J. Spectrosc. 26 (1981) 95–102.
[34] J. Milhaud, V. Ponsinet, M. Takashi, B. Michels, Interactions of the drug amphotericin B with phospholipid membranes containing or not ergosterol: new insight, into them role of ergosterol, BBA-Biomembranes 1558 (2002) 95–108.
[35] M. Herec, A. Islamov, A. Kuklin, M. Gagos, W.I. Gruszecki, Effect of antibiotic amphotericin B on structural and dynamic properties of lipid membranes formed with egg yolk phosphatidylcholine, Chem. Phys. Lipids. 147 (2007) 78–86.
[36] J. Mazerski, J. Grzybowska, E. Borowski, Influence of net charge on the aggregation and solubility behavior of amphotericin-B and its derivatives in aqueous-media, Eur. Biophys. J. 18 (1990) 159–164.
[37] D.J. Schneider, J.H. Freed, Calculating slow motional magnetic resonance spectra: a user's guide, in: L.J. Berliner, J. Reuben (Eds.), Spin Labeling. Theory and Applications, vol. 8, Plenum Press, New York, 1989, pp. 1–76.
[38] D.E. Budil, S. Lee, S. Saxena, J.H. Freed, Nonlinear-least-squares analysis of slow-motion EPR spectra in one and two dimensions using a modified Levenberg–Marquardt algorithm, J. Magn. Reson. 120 (1996) 155–189.
[39] J.H. Freed, Theory of slow tumbling ESR spectra for nitroxides, in: L.J. Berliner (Ed.), Spin Labeling: Theory and Applications, vol. 1, Academic Press, New York, 1976, pp. 53–132.
[40] B.L. Bales, Inhomogeneously broadened spin-label spectra, in: L.J. Berliner, J. Reuben (Eds.), Spin Labeling: Theory and Applications, vol. 8, Plenum Press, New York, 1989, pp. 77–130.
[41] A.G. Redfield, The theory of relaxation processes, in: J.S. Waugh (Ed.), Advances in Magnetic Resonance, vol. 1, Academic Press Inc., New York, 1965, pp. 1–32.
[42] J.H. Freed, G.K. Fraenkel, Theory of linewidths in electron spin resonance spectra, J. Chem. Phys. 39 (1963) 326.
[43] S. Schreier, C.F. Polnaszek, I.C.P. Smith, Spin labels in membranes problems in practice, Biochim. Biophys. Acta. 515 (1978) 375–436.
[44] H.J. Halpern, M. Peric, C. Yu, B.L. Bales, Rapid quantitation of parameters from inhomogeneously broadened EPR-spectra, J. Magn. Reson. 103 (1993) 13–22.
[45] L.A. Sklar, B.S. Hudson, M. Petersen, J. Diamond, Conjugated polyene fatty-acids on fluorescent-probes — spectroscopic characterization, Biochemistry-US 16 (1977) 813–819.
[46] W.L. Hubbell, H.M. Mcconnel, Molecular motion in spin-labeled phospholipids and membranes, J. Am. Chem. Soc. 93 (1971) 314.
[47] O.H. Griffith, P.J. Dehlinge, S.P. Van, Shape of hydrophobic barrier of phospholipid bilayers (evidence for water penetration in biological-membranes), J. Membr. Biol. 15 (1974) 159–192.
[48] E.L. Duarte, T.R. Oliveira, D.S. Alves, V. Micol, M.T. Lamy, On the interaction of the anthraquinone barbaloin with negatively charged DMPG bilayers, Langmuir 24 (2008) 4041–4049.
[49] J. Bolard, M. Cheron, J. Mazerski, Effect of surface curvature on the interaction of single lamellar phospholipid-vesicles with aromatic and nonaromatic heptaene antibiotics (vacidin-a and amphotericin-B), Biochem. Pharmacol. 33 (1984) 3675–3680.
[50] J. Katsaras, T.A. Harroun, J. Pencer, M.P. Nieh, "Bicellar" lipid mixtures as used in biochemical and biophysical studies, Naturwissenschaften 92 (2005) 355–366.